A Review Paper on Microscopic Modalities used in Biomedical Applications

Neeru Singla[1], Ashok Kumar[2], Himanshu Rikhari,[1] and Vishal Srivastava[3]
[1]School of Bioengineering and Biosciences, Lovely Professional University, Phagwara, Punjab, India.
[2]Electrical and Instrumentation Engineering Department, Sant Longowal Institute of Engineering and Technology, Longowal, Punjab, India
[3]Electrical and Instrumentation Engineering Department, Thapar Institute of Engineering and Technology, Patiala, Punjab, India

*Corresponding author's e-mail address: neeru.25641@lpu.co.in

<u>**Abstract**</u>

Optical microscopy is an advanced method in modern healthcare. While advances in optical microscopy allow doctors to visualize biomedical applications in unprecedented detail, the analysis of these images remains subjective, important to inter- and intra-observer discrepancy. In spite of this, conventional microscopy images capture only qualitative information which makes it difficult to automate the process, decreasing the throughput achievable in the diagnostic workflow. Nowadays, Quantitative Phase Imaging (QPI) modalities have been advanced to overcome these two challenges. By quantifying physical parameters of biomedical applications, these techniques remove subjectivity from the disease diagnosis process and allow for easier automation to increase throughput. We focus on the areas of biomedical applications, where most significant advances have been made to date.

1. INTRODUCTION

Optical microscopy is one of the standard tool for non-destructive testing of biological and industrial objects [1]. For the visualization of internal microstructure mainly in biomedical applications a high spatial resolution optical microscope with contrast agent is required [2]–[4]. In optical microscopy, contrast may be either exogenous (extrinsic) or endogenous (intrinsic). The well-known modality utilizing exogenous contrast to provide targeted morphological information is fluorescence microscopy, in which a specimen is labelled with a fluorescent molecule [5], [6]. Although, fluorescence microscopy is continuously applied across a broad range of studies, as there are number of applications in biology for which methods employing endogenous contrast are required. This is because label-free methods are not subject to photo-bleaching or photo-toxicity and therefore permit the observation of living cells in their natural environment over indefinite time periods with nearly or no sample preparation is required [7]. The main challenge associated with endogenous contrast is that cells should be transparent phase objects and produce very little contrast under normal illumination conditions. This problem has been solved optically using methods such as phase contrast (PC) [8], differential interference contrast (DIC) [9], confocal microscopic imaging, digital holographic microscopic imaging and Hoffmann modulation contrast (HMC) microscopy [10]. But all above mentioned techniques suffers some limitations either depth of penetration or with poor spatial and axial resolution. Abbe gave an idea for the phase imaging, produced by interference pattern between the scattered and the unscattered light beams, used in the above methods [8]. This information acknowledged by Zernike to develop

phase contrast microscopy [11]. Phase contrast microscopy has a potential to improve the contrast of an image by putting a quarter-wavelength delay between the reference beam and the sample beam. Phase contrast has encouraged many biological imaging studies and received Zernike in 1953 Nobel Prize in Physics [8]. While widely adopted by microscopists world-wide for label-free imaging, phase contrast images can only provide qualitative information. Nowadays, it has become clear that the quantitatively measuring the properties of cellular activities with high resolution, in three dimensions, across a wide range of spatial and temporal scales, and in a minimally invasive manner are required [12]–[14]. Multi-scale facilities are important, since the developing cellular behaviour is the outcome of taking whole information from inter-cellular interactions, intra-cellular molecular reactions and myriad environmental stimuli. The output response to these factors also has different implications at a wide range of scales. The observations of the changes at the cellular level in the growth rate, morphology, in the cell cycle, or motility or in various inter-cellular processes. Further, changes may be taken at the level of the cellular culture or population in the overall proliferation rate, spatial architecture, etc. However, to understand the behaviour of the cellular studies, there is a requirement of those measuring techniques which can enumerate all the parameters simultaneously, across the relevant spatial and temporal scales. All the above-mentioned methods are very useful but all suffers from one important drawback, that measured intensity has nonlinear, and thus non-invertible, relationship with the phase of the specimen. The field of quantitative phase imaging (QPI) was born out of attempts to quantitate the contrast generating mechanism in phase contrast microscopy. Without this information, extracting morphologically relevant parameters like size, refractive index (RI) and dry mass density, etc. are not much effective. With the help of QPI, we can extract the phase variations and RI of the specimen. Figure 1 illustrates the information which is typically available from QPI experiments [15].
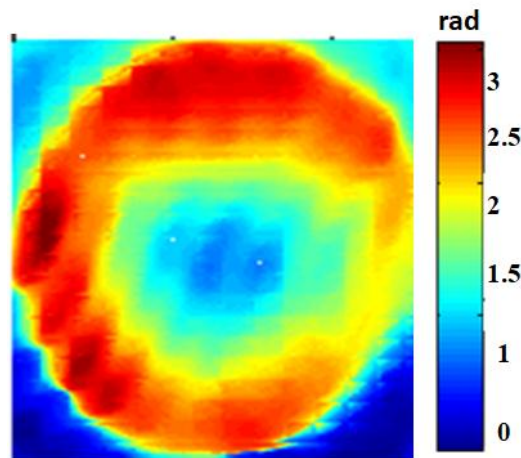
Figure 1 Representation of QPI data

2. QUANTITATIVE PHASE IMAGING

QPI provides much more rigorous analysis of the image as compare to the intensity image obtained by conventional microscopic technique. The phase map contains various information, such as cell thickness and RI which allow quantization of cellular morphology under experimental conditions [16], [17]. Nowadays, QPI play an important role in the biological studies [18], [19]. For example, QPI has recently measured cell cycle-dependent growth patterns by exploiting the fact that phase images are proportional to morphological changes like dry mass density, RI etc. [20] and brought insight to the age-old question of how single cells regulate their growth. QPI has also enabled the monitoring of

cytoskeletal/organelle interactions on short time-scales due to its ability to image cytoskeletal structures in parallel [21], whereas, fluorescence microscopy requires multiple fluorescent labels to get the same image information. Likely, QPI has been used to quantify intracellular mass transport [22], monitor the effects of Adenosine triphosphate (ATP) on red blood cell (RBC) and membrane dynamics [23]. In addition to biology, QPI is making waves in the realm of clinical diagnostics [12], [24], [25], where it has recently manifested itself as a powerful tool for low-cost, high throughput, and high-sensitivity RBC screening [26]. Another developing area for QPI is cancer diagnosis, where it has been used to differentiate cancerous cells in isolation [27], identify tissue self-affinity as a potential biomarker for precancer [28], detect calcium oxalate as a breast cancer screening tool, and correlate cancerous regions in prostate biopsies with high variance in the phase image [29].

Recently, various QPI methods have been developed to obtain the quantitative images of different biological objects such as optical coherence microscopy (OCM) [3], [30], [31], tomographic phase microscopy (TPM) [32], phase-shifting interferometry (PSI) [33], Fourier phase microscopy (FPM) [18], digital holographic microscopy (DHM) [16], diffraction phase microscopy (DPM) [34], spectroscopic diffraction phase microscopy [35] and Hilbert phase microscopy (HPM) [36]. All these methods are very much successful and each technique has its own advantages and disadvantages. QPI interferometry technique is the high-resolution quick imaging and simultaneous production of interference between the sample and reference objects.
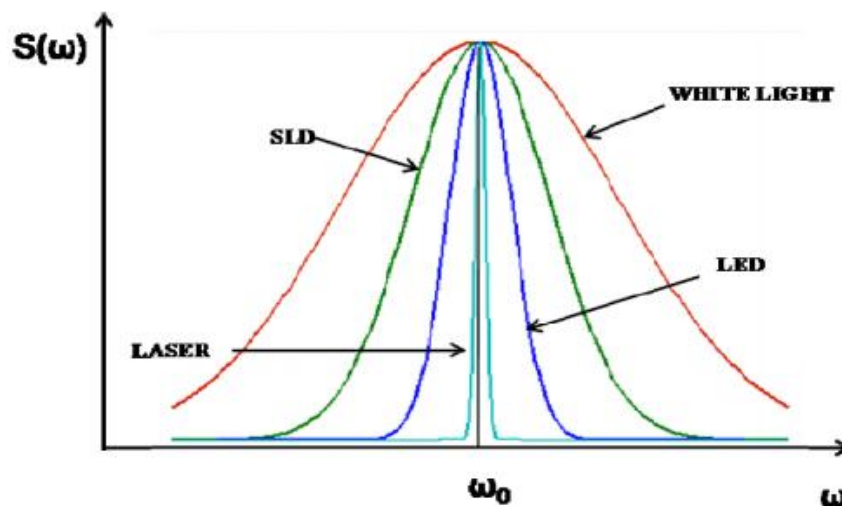
Figure 2 Optical spectrum profiles of various light sources vary with the bandwidth variation.

To optimize the image quality, the choice of light source is very critical. It is desirable to use broad band light source whose coherence length is very small to achieve better axial resolution [37]. Therefore, the unwanted fringes due to multiple reflections from the different surfaces can be avoided and accurate slice selection in the sample is possible. A qualitative comparison between the optical spectrum of a broadband source and that of a laser is shown in figure 2 [38]. The spectrum of super luminescent diode (SLD) is not always broader than light emitting diodes (LED), such as in the case of white LED. But as compare to single color LED the SLD spectrum is relatively broader bandwidth.

3. QUANTITATIVE PHASE IMAGING METHODS

QPI methods image the optical path length of a phase object integrated along the optical or z-axis. In the literature, there are numerous ways to do this [9]. QPI can be broadly classified into two categories: PSI and slightly off-axis interferometry (OAI). To understand the comparison between the QPI methods, we theoretically explain the spatial frequency domains of the methods in figure 3, slightly off-axis and PSI interferometry [39], [40].
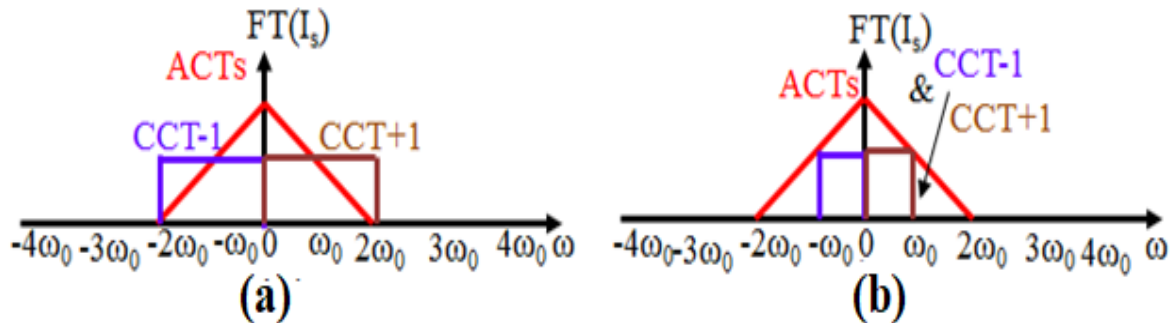
Figure 3 Graphically differentiate the spatial frequency spectrum of (a) Slightly OAI, and (b) PSI; CCT (Cross Correlation Term), ACT (Auto Correlation Term).

In both cases the two auto-correlation terms (ACTs), situated around the origin of the spatial spectrum, this consists of the reference arm and sample arm. Since the reference arm is taken to be a constant axis over the camera illumination area, the total width of the ACTs for an interferometric image is only determined by the width of the sample arm ACT given by four times the highest spatial frequency ω_0 of the object recorded by the camera. In comparison, the width of each cross-correlation term (CCT) is only   .

In slightly-OAI as seen in figure 3(a), the CCTs should not be overlapped, but the overlapping of the ACTs with each CCT's is acceptable. Therefore, the highest spatial frequency needed per exposure is only   . However, in the case of phase shifting interferometry as shown in figure 3(b) all ACTs and CCTs are centered at the origin. Therefore, the required highest spatial frequency per exposure is only ω_0. So, therefore, in this case, four or five interferogram patterns (depending on the technique chosen) should be attained to completely remove the both ACTs and one of the CCTs.

i.   Phase-Shifting Interferometry

In PSI, a coherent laser beam is incident on an imaging system/interferometer. The beam is split into sample and reference arms, which are then recombined collinearly at the image plane [41]. By modulating the phase of the reference arm, the resulting interferograms are also modulated where the bias of each pixel is determined by the phase of the sample. Conventionally, four interferograms are measured as the reference phase is modulated in equal increments around the unit circle such that the phase image is easily obtained using trigonometric relationships [14]. A block diagram representation is given in figure 4 which includes spatial filter (SF), beam splitter (BS), objective lens (OBJ) and CCD [42].
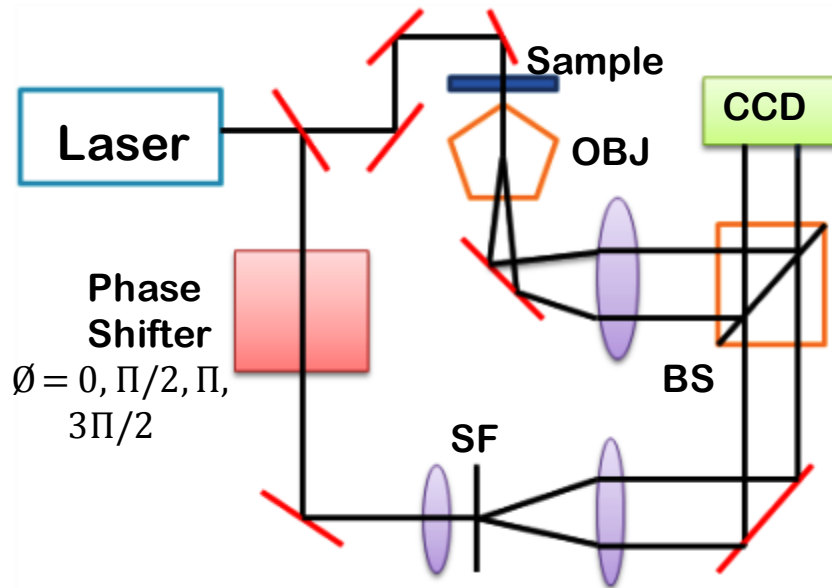
Figure 4 Schematic representation of PSI.

Because the interfering beams are collinear, PSI preserves the spatial resolution inherent in the sample arm's imaging optics, which may be diffraction-limited [9]. Phase sensitivity is determined by the Signal to Noise Ratio (SNR) which is easily maximized by controlling the relative powers of each beam. Furthermore, the method is computationally simple and requires no assumptions about the scattering properties of the sample. Disadvantages in PSI stem from the fact that multiple interferograms are required per phase image thereby limiting acquisition speed. Also, phase and speckle noise tend to reduce temporal and spatial phase stability in systems utilizing non-common-path geometries and monochromatic light. In the recent years, researchers have mitigated some of these issues by sacrificing alignment tolerance for speed [43] and adapting PSI to common-path geometries [44] and white light illumination [34].

ii.   Slightly Off-Axis Interferometry

To extract the phase information of the dynamic biological samples, since it requires only single interferogram slightly off-axis interferometry performs better as compared to PSI interferometry. Slightly-OAI is similar to PSI, except that spatial, rather than temporal, modulation is used in which the reference beam propagates at a known off-axis angle. The resulting interferograms are spatially modulated with a periodicity determined by this angle. The transmission function of the sample can be reconstructed in many ways; for example Fourier domain demodulation [4] or Hilbert transform methods [45] may be used. A block diagram representation is given in figure 5.
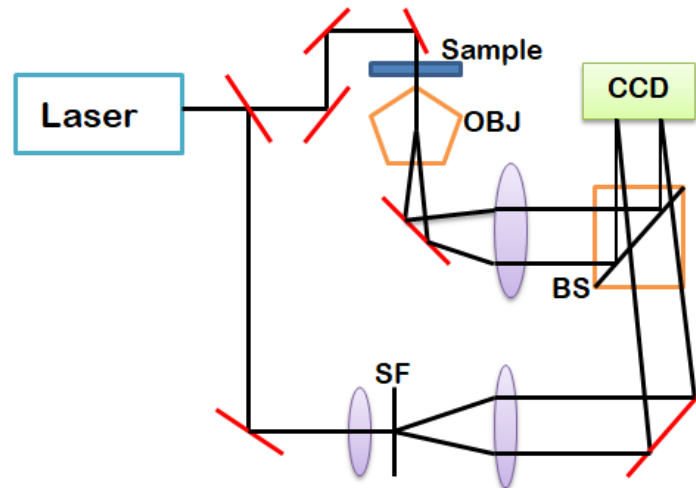
Figure 5 Schematic representation of slightly- OAI.

Because phase recovery is based on a single interferogram, temporal resolution is maximized and only limited by camera readout speed. Like PSI, slightly-OAI benefits from controllable fringe visibility and doesn't require scattering assumptions. Unlike PSI, however, spatial resolution in slightly-OAI is often limited by the off-axis angle and not the imaging optics. Slightly-OAI also suffers from reduced sensitivity associated with phase and speckle noise and reconstruction methods are often complicated by the need to unravel a highly wrapped phase function in the presence of noise [46]. As with PSI, slightly-OAI researchers have increased phase stability by adopting common-path geometries [47] and using white light [34].

iii. Quantitative Phase Imaging Method Comparison

The overall characteristics of selected QPI methods reported in the literature are summarized in Table 1. The configurations cited in Table 1 are not exhaustive and are meant to be representative of progress within each category.

Table 1 Characteristic summaries for representative QPI methods

QPI Method	Published Configuration	Single-shot	High resolution	Sensitivity	Common Path	Broadband Light Source	No object Scattering Assumptions	Computa-tionally simple
PSI	PS-DHM [16]	✗	✓	✓	✗	✗	✓	✓
	FPM [18]	✗	✓	✓	✓	✗	✓	✓
	SLIM [48]	✗	✓	✓	✓	✓	✓	✓
Slightly OAI	Slightly-OA-DHM [47]	✓	✗	✓	✗	✗	✓	✗
	DPM [49]	✓	✗	✓	✓	✗	✓	✗
	wDPM [34]	✓	✗	✓	✓	✓	✓	✗

where, ✓'s indicates presence of a desired attributes, ✗'s indicates absence of a desired attributes.

The table compares QPI methods using the following metrics: single-shot (enables high acquisition speed), high spatial resolution, sensitive (high SNR), common-path (eliminates phase noise), broadband light source (reduces speckle noise), no object scattering assumptions (strongly scattering 2D phase objects with sharp edges can be imaged without artifacts), and computationally simple (enables real-time processing). From the above table it's sufficient to motivate the present research work that we have to develop a single-shot, high resolution,

common-path broadband slightly off-axis quantitative phase microscope system to achieve higher stability and fast acquisition for biological applications.

4. OPTICAL COHERENCE TOMOGRAPHY

Optical coherence tomography (OCT) is a non-invasive medical imaging technique which is being reliable for high resolution (micrometer-scale) tomographic imaging of biological applications as well as it measures the amplitude of the backscattered light by the sample being imaged [50], [51]. OCT was initially given by Huang et.al [1] in time-domain mode of operation. The OCT can be envisioned as an optical analogy to ultrasound imaging where the technique visualizes echoes from discrepancies in a sample. In OCT, light is being used as a source for the detection of optical echoes rather than sound. OCT has many advantages like low temporal coherence property of light source for high sensitivity and high resolution optical sectioning [1], [52], [53]. Light reflected or backscattered from the object propagates with different delay times, from the different layers of the object [50]. By translating the reference mirror one can obtain a longitudinal profile of reflectivity versus depth. OCT measures the eco-time delay of back scattered or back reflected light from different layers of the object to determine the dimension of object. The key parameters in OCT systems are sensitivity, resolution and acquisition speed. Axial resolution depends upon bandwidth of the light source whereas lateral resolution depends upon the numerical aperture (NA) of the imaging optics [52].
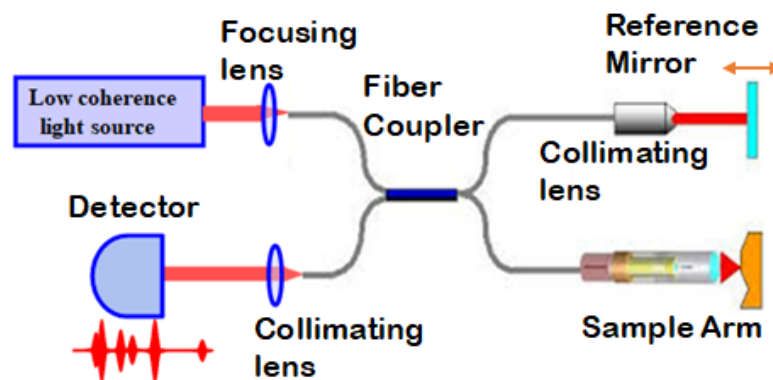
Figure 6 (a) Schematic diagram of optical coherence tomography.

The schematic diagram of a traditional OCT system is illustrated in the figure 6 (a). A fiber-coupler based Michelson interferometer is illuminated by a broad band or low coherence light source. Light is directed to 2×2 fiber coupler and it is supposed to be equal power is dispersed on both sample and reference arms, however, there are so many OCT systems which take the advantage of unbalance power splitting and have been described both experimentally and theoretically [54]. The output light at the reference fiber is incident on the reference mirror while the light at the output of the sample arm is incident onto the sample.
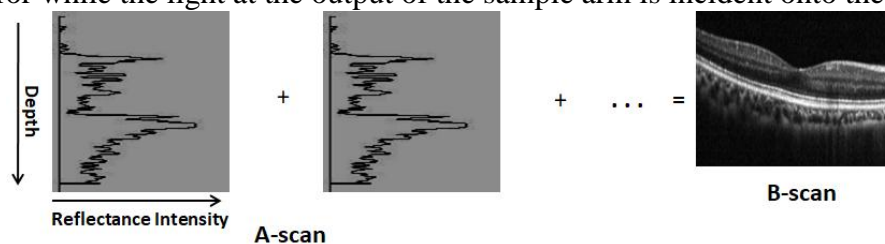
Figure 6 (b) A-scan and B-scan OCT images.

Light reflected or backscattered from the object propagates with different delay times, from the different layers of the object [19], [50] and the combined light is made to interfere on the surface of a photo-receiver or detector. By translating the reference mirror one can obtain a longitudinal profile of reflectivity versus depth, i.e. A-scan as shown in figure 6(b). On the basis of the point by point scanning mechanism the focused beam position into the sample, multiple A-scans are obtained and interfaced in the desktop into a 2D cross-sectional image of the sample in the region of the focal spot, defined as B-scan shown in figure 6(b) [1].

i. Theoretical Aspects of Extraction of Signal using OCT

From the figure 7, if a wavelength-independent bifurcation ratio for the beam splitter is taken, then the electric fields for low coherent light source reflected into sample and reference beams of the interferometer can be expressed as [38]:

$$E_S = E_R = b(k)e^{-j(\omega t - kz)} \tag{1}$$

where, E_R is the electric field at the reference beam,

E_S is the electric field at the sample beam,

$b(k)$ is the electric field amplitude spectrum,

k is the wave-number,

and z is the distance from the different layers of the sample.

Therefore, the attenuated electric field of the reference beam is as follows:

$$E_R = r_R b(k)e^{-j(\omega t - 2kz_R)} \tag{2}$$

where, r_R is the reference beam.

$$I_{det}(k) = \frac{\delta}{2}\left(I_R + \left(E_S E_S^*\right) + 2\operatorname{Re}\left\{\left(E_R E_R^*\right)\right\}\right)$$
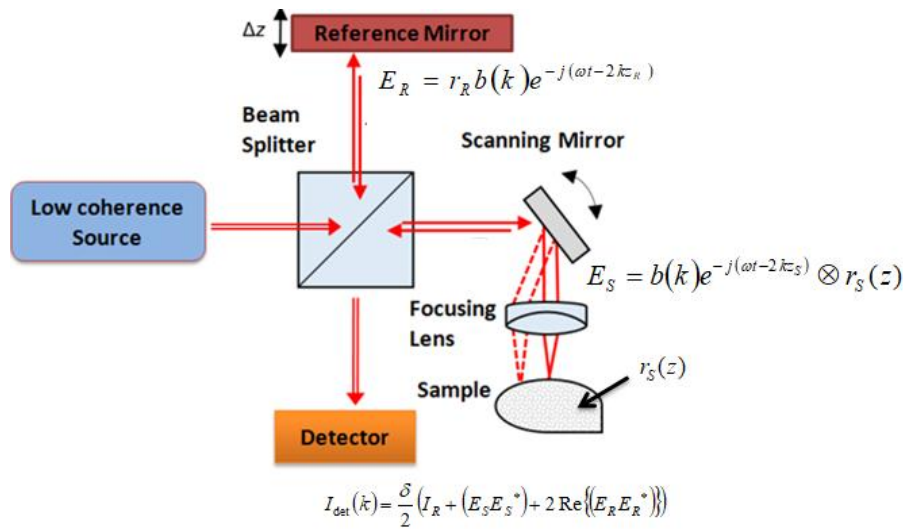
Figure 7 Schematic diagram of conventional OCT

The light incident on any given specimen will undergo back reflected from the multiple layers due to the presence of scattering particles and refractive index variations within the specimen. The back reflected photons reoccurring from the sample beam can be expressed by:

$$E_S = b(k)e^{-j(\omega t - 2kz_S)} \otimes r_S(z) \tag{3}$$

where, $r_S(z)$ is the depth-dependent amplitude reflectivity function of any given specimen.

Therefore, the sample and reference beams are recombined at the beam splitter and are given as,

$$E_{\det} = \frac{1}{\sqrt{2}}\left(E_S + E_R\right) \tag{4}$$

The incident light in terms of electric field is converted to photo current with the help of optical detectors, which are based on square law intensity detection devices. So, the originated photo current is directly related to the product of the average time of the incident electric field and its complex conjugate which is as follows:

$$I_{\det}(k) = \frac{\delta}{2}\left(E_S + E_R\right)\left(E_S{}^* + E_R{}^*\right) = \frac{\delta}{2}\left(I_R + \left(E_S E_S{}^*\right) + 2\operatorname{Re}\left\{\left(E_R E_R{}^*\right)\right\}\right) \tag{5}$$

where, δ is the detector responsivity in Ampere/Watt. The right-hand side of the first two term of the equation correspond to the DC component of the current and interference generated within the given specimen. The final term of the equation 5 represents the interference pattern generated between the reference and sample beams which further utilized to compute the structural information or axial depth profile in OCT. When the signal was simplified, the AC component of the photocurrent can be expressed as:

$$I_{ac}(k,\Delta z) = \delta B(k)\sqrt{R_R} R_S(\Delta z)\cos\left[2k\Delta z\right] \tag{6}$$

In order to obtain the axial structural profile information, the depth-dependent reflectivity function $R_S(\Delta z)$ of any desired specimen is extracted using various OCT signal processing techniques. In a point by point scanning system, the light propagates from the interferometer and is directly send to a detector is illustrate in figure 7. After taking the resampling and subtraction of the DC background, the axial depth profile of the structural information is produced by performing the inverse Fourier transform process. Different types of OCT are used to study the biological and industrial objects non-invasively [55]–[58].

ii.   Categories of Optical Coherence Tomography
OCT can be broadly divided into two main categories: time domain OCT (TD-OCT) and Fourier or frequency domain OCT (FD-OCT). In TD-OCT, the autocorrelation gives information about source spectral distribution. In contrast, in FD-OCT, the autocorrelation is calculated by the Fourier transform of the power spectral signal that is measured directly.

iii.   Time-Domain Optical Coherence Tomography (TD-OCT)
In time-domain OCT, the wavenumber - dependent photo detector current is recorded with the help of a single or multiple detectors where the reference beam is used to match the optical path length from the different depth reflections within the sample [52], [59]. To acquire the depth profile in TD-OCT reference mirror is moved in axial direction or in the direction of wave propagation to map out the sample reflectivity as a function of axial depth. Figure 8 shows the schematic diagram of TD-OCT system based on Michelson interferometer. The system uses a broad band light source. The light coming out from the source has been divided into two parts with the help of 2x2 fiber, one part is going towards the reference mirror and other part towards sample arm. The light reflected from the sample and the light reflected from the reference arm again recombines at fiber coupler. When the path difference between the reference arm and object arm is within the coherence length of light source interference occurs and recorded by the detector. Due to mechanical movement

of the reference mirror to obtain the sample depth profile it gives rise to motion artifacts and limited repeatability [52].
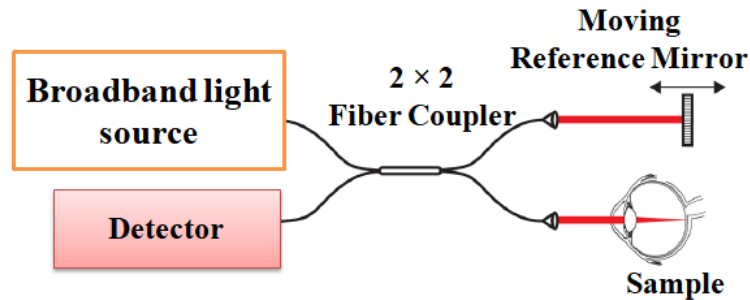
Figure 8 Schematic diagram of TD-OCT.

iv.   Fourier Domain Optical Coherence Tomography (FD-OCT)

In FD-OCT, signal detection relies on the transformation of the OCT time-varying signal along the optical axis, termed the A-scan, into the frequency domain. Thus FD-OCT has an advantage that full sample depth information can be extracted without scanning the reference mirror. FD-OCT was first introduced by A. F. Fercher, et al. in 1995 [60]. In 2003, R. Leitgeb et al. [61] and M. A. Choma et al. [53] showed that FD-OCT techniques provide sensitivities two to three orders of magnitude greater than TD-OCT. This sensitivity advantage would enable imaging hundreds of times faster than TD-OCT without sacrificing image quality. This dramatic improvement in imaging speeds in frequency domain detection made acquisition of 3D data sets feasible [61]. To analyze the spectrum of the interference signal in FD-OCT, in which the depth of the layer represents the frequency component and the reflectivity of that layer represents the amplitude [62]. Still, FD-OCT has also certain limitations. In FD-OCT, the optical frequency components yielded by the interferometer consists of two symmetrical components, they are complex conjugate to each other and called mirroring effect. The basic principle behind FD-OCT is Wolf's solution to the inverse scattering problem for determining the structure of weakly scattering objects.
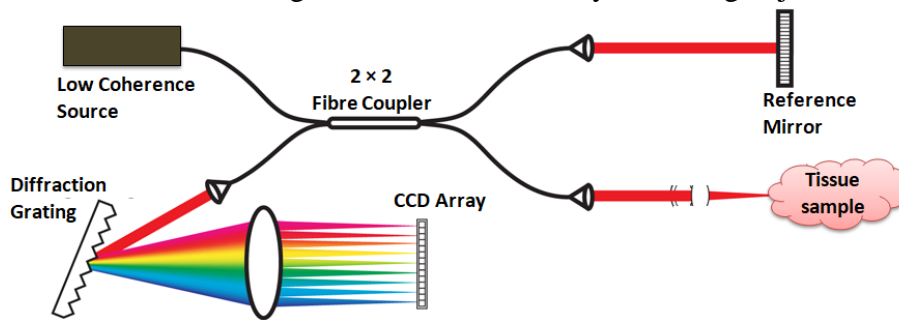
Figure 9 Schematic diagram of SD-OCT system [4].
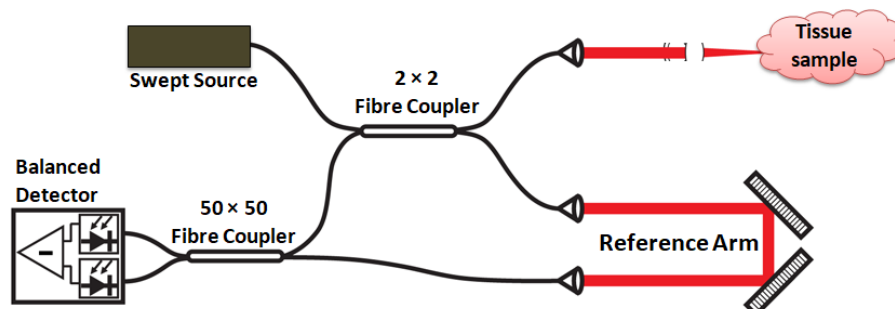
Figure 10 Schematic diagram of SS-OCT system [64].

According to the Winner-Khintchine theorem, the spectral power amplitude of backreflected beam equals to the Fourier transform of the axial distribution of the object scattering potential [63]. Based on its implementation, the FD-OCT can be split into further two types: Spectral Domain OCT (SD-OCT) and Swept-Source OCT (SS-OCT). SD-OCT consists of a broadband light source and a spectrometer used in the detector arm to acquire the interference signal from the deep layers of the sample as seen in figure 9 [4]. The interference signal is dispersed by the diffraction grating and the corresponding to each individual wavelength components are detected by a CCD array. However, SS-OCT using a high speed tunable, narrow line width laser source and without dispersion components as seen in figure 10 [61]. In SS-OCT system, the given sample is probed with a narrow band instead of sampling the received spectrum over a finite wavelength.

v. Full-Field Optical Coherence Tomography (FF-OCT)

FF-OCT system is a technology extension of point-by-point scanning OCT system. In conventional OCT system we need three mechanical scan (one depth and two lateral scans) which will produce motion artifacts, non-repeatability and time-consuming [52]. FF-OCT system draws a lot of attention since it produces *enface* images and potentially faster operations. The basic principle behind the FF-OCT is low coherence interferometry. It uses low temporal and spatial coherence light source. In FF-OCT system a point detector is replaced by a 2D array of detector. The major parameters to perform full field OCT (FF-OCT) is the detector array used to detect the interference fringe pattern which classifying the OCT signal. In FF-OCT, the process of coherence detection is carried out in parallel at all the pixels. The transverse resolution of FF-OCT is similar to conventional microscopy whereas the axial resolution is determined by the spectral properties of the illumination source. Thus FF-OCT is an alternative approach to increase the imaging speed and acquire the larger area or full-field by an array of detector, such as, charged couple device (CCD) or complementary metal oxide semiconductor (CMOS) camera [31], [65]. Recently, the use of FF-OCT has been increased as a non-scanning, high resolution en-face imaging methods in several biological applications [66]–[69]. A schematic diagram of the FF-OCT based on Linnik interference microscope configuration which consists of beam splitter (BS), microscope objective (MO), neutral density filter (NDF), window glass (WG), angled mirror (AM), piezo-electric transducer (PZT), reference mirror (RM), collimating lens (coll lens) and 2D-CCD are shown in figure 11. Parallel acquisition allows simplification of the framework just as a higher acquisition speed as compare to point by point scanning OCT [39], [70].
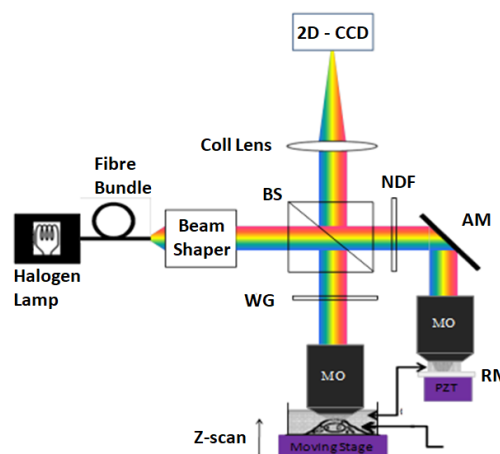
Figure 11 Schematic diagram of the FF-OCT system [71].

. Moreover, FF-OCT offers the likelihood to utilize thermal light sources regardless of their low brightness by exploiting the much slower axial scan than in point scanning OCT [3], [72]. However, the brightness of thermal light sources remains insufficient requiring a trade-off between sensitivity and acquisition speed [73]. In FF-OCT, owing to a natural broad spectrum, a thermal light source offers a micrometer resolution along with the more benefits of low cost and simplicity. OCT, image acquisition depends on a detector array. In parallel TD-OCT techniques, the transverse en-face images can be obtained by utilizing full-field illumination and 2D area scan detector, referred as FF-OCT [30], [70]. Various FF-OCT frameworks have been employed utilizing 2D smart pixel silicon detector arrays [70] and CCD cameras [65], but in these frameworks for obtaining the depth structure of a sample the axial mechanical scanning of the reference arm must be performed.

5. APPLICATIONS OF OCT

OCT have been widely investigated in clinical diagnosis to detect the different types of diseases [74]–[78]. OCT is a young imaging modality that is still under process to find the better role play in the current medical applications [79]–[81]. During the past decades, OCT has become a suitable tool for developing high resolution, cross-sectional images in the biomedical field [52], [55], [82], [83]. The high spatial resolution allows precise investigations of both interior imaging and surface topography of any specimen. However, with the conventional methods used fiber coupler for sending and collecting the light, OCT can easily introduce into catheters and endoscopes and have been developed for intraluminal imaging [50], [84]. Further, OCT is also an important analytical tool for other biomedical applications like in developmental biology, cardiology, laryngology, gastroenterology, pulmonary medicine, dermatology, dentistry, etc. [14], [55], [85], [86]. Their histological data are evaluated by OCT, functioning as the optical biopsy to make a fast diagnosis at endoscopy. Previously, this was only feasible by using histological or cytological analysis, which is having a big problem to remove the tissue sample and processing for microscopic examination [87]–[89]. Various techniques have been successfully used for disease diagnosis and wide aspects of biomedical area [90-101]. Usually, it's a time-consuming process for the image examines manually which is very common in clinical applications. In addition, there is dependably a subjective factor related to the pathological examination of an image that builds the potential hazard for a specialist to make a false decision. In this manner, an automated framework will give important assistance to doctors. With the help of image analysis and machine learning algorithms, this research work plan to design reliable diagnostic models for analysing the medical image data to reduce the difficulties faced by medical specialists in image assessment.

6. CONCLUSIONS

In summary, the various optical microscopic modalities were discussed in this paper which are having major contribution in biomedical applications. In addition to providing quantitative information, QPI techniques are also label-free and user friendly into the current diagnostics. In this paper, we review the advance methods made in biomedical applications by QPI techniques.

REFERENCES
[1]   Huang, D et al. (1991). Optical coherence tomography. S*cience*, *254*(5035), 1178-1181.
[2]   Popescu, D. P et al. (2011). Optical coherence tomography: fundamental principles, instrumental designs and biomedical applications. *Biophysical reviews*, *3*(3), 155.
[3]   Grieve, K et al. (2005, April). Full-field OCT: ex vivo and in vivo biological imaging

applications. In *Coherence Domain Optical Methods and Optical Coherence Tomography in Biomedicine IX* (Vol. 5690, pp. 31-39). International Society for Optics and Photonics.

[4]   Sarunic, M. V., Applegate, B. E., & Izatt, J. A. (2005). Spectral domain second-harmonic optical coherence tomography. *Optics letters*, *30*(18), 2391-2393.

[5]   McLaughlin, R. A., Lorenser, D., & Sampson, D. D. (2013). Needle probes in optical coherence tomography. *Handbook of Coherent-Domain Optical Methods: Biomedical Diagnostics, Environmental Monitoring, and Materials Science*, 1065-1102.

[6]   Chowdhury, S., & Izatt, J. A. (2016, April). Simultaneous fluorescence and phase imaging with extensions toward sub-diffraction resolution via structured-illumination (Conference Presentation). In *Three-Dimensional and Multidimensional Microscopy: Image Acquisition and Processing XXIII* (Vol. 9713, p. 97131J). International Society for Optics and Photonics.

[7]   Kemper, B., Langehanenberg, P., & Bauwens, A. (2013). Holographic Microscopy Techniques for Multifocus Phase Imaging of Living Cells. In *Biomedical Optical Phase Microscopy and Nanoscopy* (pp. 97-128). Academic Press.

[8]   Zernike, F. (1942). Phase contrast, a new method for the microscopic observation of transparent objects part II. *Physica*, *9*(10), 974-986.

[9]   Kraut, S., & Cowley, J. M. (1993). A simplified mode of differential phase contrast Lorentz microscopy. *Microscopy research and technique*, *25*(4), 341-345.

[10]   Hoffman, R., & Gross, L. (1975). Modulation contrast microscope. *Applied Optics*, *14*(5), 1169-1176.

[11]   Zernike, F. (1955). How I discovered phase contrast. *Science*, *121*(3141), 345-349.

[12]   Pham, H. V. et al. (2013). Real time blood testing using quantitative phase imaging. *PloS one*, *8*(2), e55676.

[13]   Rosen, J., & Takeda, M. (2000). Longitudinal spatial coherence applied for surface profilometry. *Applied optics*, *39*(23), 4107-4111.

[14]   Popescu, G. (2011). *Quantitative phase imaging of cells and tissues*. McGraw Hill Professional.

[15]   Singla, N., Srivastava, V., & Mehta, D. S. (2018). Development of full- field optical spatial coherence tomography system for automated identification of malaria using the multilevel ensemble classifier. *Journal of biophotonics*, *11*(5), e201700279.

[16]   Yamaguchi, I., & Zhang, T. (1997). Phase-shifting digital holography. *Optics letters*, *22*(16), 1268-1270.

[17]   Yoon, S. K et al. (2007). Phase Unwrapping using Modified Goldstein Algorithm in Digital Holography. *Korean Journal of Optics and Photonics*, *18*(2), 122-129.

[18]   Popescu, G et al. (2004). Fourier phase microscopy for investigation of biological structures and dynamics. *Optics letters*, *29*(21), 2503-2505.

[19]   Tearney, G. J et al. (1996). Rapid acquisition of in vivo biological images by use of optical coherence tomography. *Optics letters*, *21*(17), 1408-1410.

[20]   Aknoun, S et al. (2015). Living cell dry mass measurement using quantitative phase imaging with quadriwave lateral shearing interferometry: an accuracy and sensitivity discussion. *Journal of biomedical optics*, *20*(12), 126009.

[21]   Popescu, G et al. (2008). Imaging red blood cell dynamics by quantitative phase microscopy. *Blood Cells, Molecules, and Diseases*, *41*(1), 10-16.

[22]   Jung, J et al. (2016). Optical characterization of red blood cells from individuals with sickle cell trait and disease in Tanzania using quantitative phase imaging. *Scientific reports*, *6*, 31698.

[23]   Park, Y et al. (2011, February). Metabolic remodeling of the human red blood cell membrane measured by quantitative phase microscopy. In *Imaging, Manipulation, and Analysis of Biomolecules, Cells, and Tissues IX* (Vol. 7902, p. 79021M). International

Society for Optics and Photonics.

[24]   Lee, K et al. (2013). Quantitative phase imaging techniques for the study of cell pathophysiology: from principles to applications. *Sensors*, *13*(4), 4170-4191.

[25]   Bhaduri, B et al. (2013) Real - time quantitative phase imaging in biomedicine. *SPIE Newsroom*, 1–5.

[26]   Cho, S et al. (2012). Optical imaging techniques for the study of malaria. *Trends in biotechnology*, *30*(2), 71-79.

[27]   Majeed, H et al. (2015). Breast cancer diagnosis using spatial light interference microscopy. *Journal of biomedical optics*, *20*(11), 111210.

[28]   Sridharan, S et al. (2015). Prediction of prostate cancer recurrence using quantitative phase imaging. *Scientific reports*, *5*, 9976.

[29]   Nguyen, T et al. (2015, March). Prostate cancer diagnosis using quantitative phase imaging and machine learning algorithms. In *Quantitative Phase Imaging* (Vol. 9336, p. 933619). International Society for Optics and Photonics.

[30]   Beaurepaire, E. et al. (1998). Full-field optical coherence microscopy. *Optics letters*, *23*(4), 244-246.

[31]   Vabre, L., Dubois, A., & Boccara, A. C. (2002). Thermal-light full-field optical coherence tomography. *Optics letters*, *27*(7), 530-532.

[32]   Kuś, A et al. (2014). Tomographic phase microscopy of living three-dimensional cell cultures. *Journal of biomedical optics*, *19*(4), 046009.

[33]   Singh Mehta, D., & Srivastava, V. (2012). Quantitative phase imaging of human red blood cells using phase-shifting white light interference microscopy with colour fringe analysis. *Applied Physics Letters*, *101*(20), 203701.

[34]   Kim, T et al. (2014). White-light diffraction tomography of unlabelled live cells. *Nature Photonics*, *8*(3), 256.

[35]   Park, Y et al. (2009). Spectroscopic phase microscopy for quantifying hemoglobin concentrations in intact red blood cells. *Optics letters*, *34*(23), 3668-3670.

[36]   Popescu, G et al. (2005). Erythrocyte structure and dynamics quantified by Hilbert phase microscopy. *Journal of biomedical optics*, *10*(6), 060503.

[37]   Ogien, J., & Dubois, A. (2016). High-resolution full-field optical coherence microscopy using a broadband light-emitting diode. *Optics express*, *24*(9), 9922-9931.

[38]   Fujimoto, J. G., & Drexler, W. (2015). Optical coherence tomography: technology and applications.

[39]   Watanabe, Y., Yamada, K., & Sato, M. (2006). In vivo non-mechanical scanning grating-generated optical coherence tomography using an InGaAs digital camera. *Optics communications*, *261*(2), 376-380.

[40]   Guo, R. et al. (2014). LED-based digital holographic microscopy with slightly off-axis interferometry. *Journal of Optics*, *16*(12), 125408.

[41]   Thomas, L et al. (2015). Phase-sharing using a Mach–Zehnder interferometer. *Applied optics*, *54*(4), 699-706.

[42]   Krauter, J et al. (2015, June). Full-field swept-source optical coherence tomography with phase-shifting techniques for skin cancer detection. In *Optical Methods for Inspection, Characterization, and Imaging of Biomaterials II*(Vol. 9529, p. 952913). International Society for Optics and Photonics.

[43]   Medoff, B. P et al. (1983). Iterative convolution backprojection algorithms for image reconstruction from limited data. *JOSA*, *73*(11), 1493-1500.

[44]   Kadono, H., Ogusu, M., & Toyooka, S. (1994). Phase shifting common path interferometer using a liquid-crystal phase modulator. *Optics communications*, *110*(3-4), 391-400.

[45]   Na, J et al. (2008). Image restoration method based on Hilbert transform for full-

field optical coherence tomography. *Applied optics*, *47*(3), 459-466.

[46]   Xue, L., Lai, J. C., & Li, Z. H. (2010, November). Quantitative phase microscopy of red blood cells with slightly-off-axis interference. In *Optics in Health Care and Biomedical Optics IV* (Vol. 7845, p. 784505). International Society for Optics and Photonics.

[47]   Cuche, E., Marquet, P., & Depeursinge, C. (2000). Spatial filtering for zero-order and twin-image elimination in digital off-axis holography. *Applied optics*, *39*(23), 4070-4075.

[48]   Wang, Z et al. (2011). Spatial light interference microscopy (SLIM). *Optics express*, *19*(2), 1016-1026.

[49]   Popescu, G et al. (2006). Diffraction phase microscopy for quantifying cell structure and dynamics. *Optics letters*, *31*(6), 775-777.

[50]   Fujimoto, G. J et al. (1995). Optical biopsy and imaging using optical coherence tomography. *Nature Medicine, 1,* 970-972.

[51]   Tomlins, P. H., & Wang, R. K. (2005). Theory, developments and applications of optical coherence tomography. *Journal of Physics D: Applied Physics*, *38*(15), 2519.

[52]   Subhash, H. M. (2012). Full-field and single-shot full-field optical coherence tomography: A novel technique for biomedical imaging applications. *Advances in Optical Technologies*, *2012*.

[53]   Choma, M. A et al. (2003). Sensitivity advantage of swept source and Fourier domain optical coherence tomography. *Optics express*, *11*(18), 2183-2189.

[54]   Chang, S et al. (2008). Large area full-field optical coherence tomography and its applications. *Open Opt. J.*, *2*(1), 10-20.

[55]   Burcheri-Curatolo, A. (2012). *Advances of full-field optical coherence tomography (FFOCT) for clinical applications and developmental biology* (Doctoral dissertation, Université Pierre et Marie Curie-Paris VI).

[56]   Zysk, A. M et al. (2007). Optical coherence tomography: a review of clinical development from bench to bedside. *Journal of biomedical optics*, *12*(5), 051403.

[57]   Choi, W. (2012). Tomographic phase microscopy and its biological applications. *3D Research*, *3*(4), 5.

[58]   Jung, W et al. (2005). Advances in oral cancer detection using optical coherence tomography. *IEEE Journal of Selected Topics in Quantum Electronics*, *11*(4), 811-817.

[59]   Watanabe, Y., Yamada, K., & Sato, M. (2006). Three-dimensional imaging by ultrahigh-speed axial-lateral parallel time domain optical coherence tomography. *Optics express*, *14*(12), 5201-5209.

[60]   Fercher, A. F et al. (1995). Measurement of intraocular distances by backscattering spectral interferometry. *Optics communications*, *117*(1-2), 43-48.

[61]   Leitgeb, R., Hitzenberger, C. K., & Fercher, A. F. (2003). Performance of fourier domain vs. time domain optical coherence tomography. *Optics express*, *11*(8), 889-894.

[62]   Liu, X et al. (2008). Fiber-optic Fourier-domain common-path OCT. *Chinese Optics Letters*, *6*(12), 899-901.

[63]   Ryabukho, V. P., et al. (2013). Wiener–Khintchin theorem for spatial coherence of optical wave field. *Journal of Optics*, *15*(2), 025405.

[64]   Fergusson, J et al. (2010, February). In vitro retinal imaging with full field swept source optical coherence tomography. In *Optical Coherence Tomography and Coherence Domain Optical Methods in Biomedicine XIV* (Vol. 7554, p. 75540I). International Society for Optics and Photonics.

[65]   Akiba, M., Chan, K. P., & Tanno, N. (2003). Full-field optical coherence tomography by two-dimensional heterodyne detection with a pair of CCD cameras. *Optics letters*, *28*(10), 816-818.

[66]   Dubois, A., & Boccara, A. C. (2008). Full-field optical coherence tomography. In *Optical Coherence Tomography* (pp. 565-591). Springer, Berlin, Heidelberg.

[67]   Popescu, G et al. (2006, October). Red Blood Cell Fluctuations During Osmolarity Changes. In *Frontiers in Optics* (p. FTuE1). Optical Society of America.

[68]   Anna, T et al. (2011). High-resolution full-field optical coherence microscopy using a Mirau interferometer for the quantitative imaging of biological cells. *Applied optics*, *50*(34), 6343-6351.

[69]   Federici, A., & Dubois, A. (2015). Full-field optical coherence microscopy with optimized ultrahigh spatial resolution. *Optics letters*, *40*(22), 5347-5350.

[70]   Ducros, M et al. (2002). Parallel optical coherence tomography in scattering samples using a two-dimensional smart-pixel detector array. *Optics Communications*, *202*(1-3), 29-35.

[71]   Yu, L., & Kim, M. K. (2004). Full-color three-dimensional microscopy by wide-field optical coherence tomography. *Optics express*, *12*(26), 6632-6641.

[72]   Boccara, A et al. (2007, October). Full-field optical coherence tomography (OCT) and early alterations in chloroplast morphology. In *Advanced Environmental, Chemical, and Biological Sensing Technologies V* (Vol. 6755, p. 67550E). International Society for Optics and Photonics.

[73]   Chinn, S. R., Swanson, E. A., & Fujimoto, J. G. (1997). Optical coherence tomography using a frequency-tunable optical source. *Optics letters*, *22*(5), 340-342.

[74]   Hussain, Z et al. (2017). Differential data augmentation techniques for medical imaging classification tasks. In *AMIA Annual Symposium Proceedings*(Vol. 2017, p. 979). American Medical Informatics Association.

[75]   Lu, G., & Fei, B. (2014). Medical hyperspectral imaging: a review. *Journal of biomedical optics*, *19*(1), 010901.

[76]   Kuo, W. C et al. (2008). Assessment of arterial characteristics in human atherosclerosis by extracting optical properties from polarization-sensitive optical coherence tomography. *Optics Express*, *16*(11), 8117-8125.

[77]   Kuo, W. C et al. (2017). In vivo images of the epidural space with two-and three-dimensional optical coherence tomography in a porcine model. *PloS one*, *12*(2), e0172149.

[78]   Singh, J., Kumar, S., & Arora, A. S. (2018). Thermographic evaluation of mindfulness meditation using dynamic IR imaging. *Infrared Physics & Technology*, *95*, 81-87.

[79]   Alonso-Caneiro, D et al. (2016). Tissue thickness calculation in ocular optical coherence tomography. *Biomedical optics express*, *7*(2), 629-645.

[80]   Singla, N., Srivastava, V., & Mehta, D. S. (2018). In vivo classification of human skin burns using machine learning and quantitative features captured by optical coherence tomography. *Laser Physics Letters*, *15*(2), 025601.

[81]   Sullivan, A. C., Hunt, J. P., & Oldenburg, A. L. (2011). Fractal analysis for classification of breast carcinoma in optical coherence tomography. *Journal of biomedical optics*, *16*(6), 066010.

[82]   Marschall, S et al. (2011). Optical coherence tomography—current technology and applications in clinical and biomedical research. *Analytical and bioanalytical chemistry*, *400*(9), 2699-2720.

[83]   Farhat, G et al. (2011, February). Optical coherence tomography speckle decorrelation for detecting cell death. In *Biomedical Applications of Light Scattering V* (Vol. 7907, p. 790710). International Society for Optics and Photonics.

[84]   Atif, M et al. (2011). Catheters for optical coherence tomography. *Laser Physics Letters*, *8*(9), 629-646.

[85]   Peters, I. T et al. (2016). Noninvasive detection of metastases and follicle density in ovarian tissue using full-field optical coherence tomography. *Clinical Cancer Research*, *22*(22), 5506-5513.

[86]   Levine, A., Wang, K., & Markowitz, O. (2016). Optical Coherence Tomography for Skin Cancer Screening. *Gavin J Dermatol Res Ther*, *2016*, 24-25.

[87]   He, L et al. (2012). Histology image analysis for carcinoma detection and grading. *Computer methods and programs in biomedicine*, *107*(3), 538-556.

[88]   Gurfinkel, R et al. (2010). Histological assessment of tangentially excised burn eschars. *Canadian Journal of Plastic Surgery*, *18*(3), 33-36.

[89]   Gurcan, M. N et al. (2009). Histopathological image analysis: A review. *IEEE reviews in biomedical engineering*, *2*, 147.

[90]   Singh J., Singh R., Singh H. Dimensional accuracy and surface finish of biomedical implant fabricated as rapid investment casting for small to medium quantity production. Journal of Manufacturing Processes, 25, 2017.

[91]   Bhati S.K., Singh O., Sunkaria R.K. Beat detection algorithm for ECG and arterial blood pressure waveforms using empirical mode decomposition: A unified approach. International Journal of Signal and Imaging Systems Engineering, 8(1-2), 2015.

[92]   Tomar A.S., Tak G.K., Chaudhary R. Image based authentication with secure key exchange mechanism in cloud. 2014 International Conference on Medical Imaging, m-Health and Emerging Communication Systems, MedCom 2014.

[93]   Mendiratta N., Tripathi S.L., Padmanaban S., Hossain E. Design and analysis of heavily doped n+ pocket asymmetrical junction-less double gate Mosfet for biomedical applications. Applied Sciences (Switzerland), 10(7), 2020.

[94]   Prakash C., Singh S., Sharma S., Singh J., Singh G., Mehta M., Mittal M., Kumar H. Fabrication of low elastic modulus $Ti_{50}Nb_{30}HA_{20}$ alloy by rapid microwave sintering technique for biomedical applications. Materials Today: Proceedings,21,2020.

[95]   Singh S., Prakash C., Wang H., Yu X.-F., Ramakrishna S. Plasma treatment of polyether-ether-ketone: A means of obtaining desirable biomedical characteristics. European Polymer Journal,118, 2019.

[96]   Singh S., Prakash C., Ramakrishna S. 3D printing of polyether-ether-ketone for biomedical applications. European Polymer Journal, 114,2019.

[97]   Kaur M., Sudhakar K., Mishra V. Fabrication and biomedical potential of nanogels: An overview. International Journal of Polymeric Materials and Polymeric Biomaterials, 68(6), 2019.

[98]   Pradhan S., Maity K., Singh S., Prakash C. Micro-machining performance assessment of Ti-based biomedical alloy: A finite element case study. Biomanufacturing, 2019.

[99]   Mann G.S., Singh L.P., Kumar P., Singh S., Prakash C. On briefing the surface modifications of polylactic acid: A scope for betterment of biomedical structures, Journal of Thermoplastic Composite Materials, 2019.

[100]   Patil A., Mishra V., Thakur S., Riyaz B., Kaur A., Khursheed R., Patil K., Sathe B. Nanotechnology derived nanotools in biomedical perspectives: An update. Current Nanoscience, 15(2), 2019.

[101]   Mishra V., Singh G., Yadav N., Barnwal R.P., Singla N., Prabhu K.I., Suttee A. Biomedical potential of graphene oxide based nanoformulations: An overview. International Journal of Drug Delivery Technology, 9(1), 2019.